The El Niño–Southern Oscillation and wetland methane interannual variability

E. L. Hodson,[1] B. Poulter,[1] N. E. Zimmermann,[1] C. Prigent,[2] and J. O. Kaplan[3]

[1] Global measurements of atmospheric methane (CH_4) concentrations continue to show large interannual variability whose origin is only partly understood. Here we quantify the influence of the El Niño–Southern Oscillation (ENSO) on wetland CH_4 emissions, which are thought to be the dominant contributor to interannual variability of the CH_4 sources. We use a simple wetland CH_4 model that captures variability in wetland extent and soil carbon to model the spatial and temporal dynamics of wetland CH_4 emissions from 1950–2005 and compare these results to an ENSO index. We are able to explain a large fraction of the global and tropical variability in wetland CH_4 emissions through correlation with the ENSO index. We find that repeated El Niño events throughout the 1980s and 1990s were a contributing factor towards reducing CH_4 emissions and stabilizing atmospheric CH_4 concentrations. An increase in emissions from the boreal region would likely strengthen the feedback between ENSO and interannual variability in global wetland CH_4 emissions. Our analysis emphasizes that climate variability has a significant impact on wetland CH_4 emissions, which should be taken into account when considering future trends in CH_4 sources. **Citation:** Hodson, E. L., B. Poulter, N. E. Zimmermann, C. Prigent, and J. O. Kaplan (2011), The El Niño–Southern Oscillation and wetland methane interannual variability, *Geophys. Res. Lett.*, *38*, L08810, doi:10.1029/2011GL046861.

1. Introduction

[2] Methane (CH_4) is an important greenhouse gas and contributes significantly to the change in global mean surface temperature both through direct and indirect radiative forcing [*Shindell et al.*, 2009]. Over the last two decades, the rate of increase of CH_4 has slowed and fluctuated with large interannual variability [*Rigby et al.*, 2008; *Dlugokencky et al.*, 2009], which is only partially understood.

[3] Inverse estimates attribute 50–70% of total global interannual variability in CH_4 emissions to wetlands [*Bousquet et al.*, 2006; *Chen and Prinn*, 2006]. This interannual variability has been connected to variations in temperature, water table depth, and precipitation [*Walter et al.*, 2001; *Bloom et al.*, 2010; *Ringeval et al.*, 2010]; however, the influence of ENSO on wetland emission variability has remained largely unstudied. ENSO has been linked to variations in CH_4 emissions from biomass burning [*van der Werf et al.*, 2006],

and is considered the major source of variability in CO_2 emissions from the land surface [*Zeng et al.*, 2005].

[4] Here we examine the effects of ENSO on wetland CH_4 emissions from 1950–2005 by using a simple wetland model based on a dynamic global vegetation model in combination with hind-casted satellite observations of wetland extent. We correlate the resulting time series with an ENSO index and analyze the spatial and temporal effects of ENSO on variability in wetland CH_4 emissions.

2. Methods

[5] We estimate natural wetland CH_4 emissions as a linear function of wetland extent (S) and heterotrophic respiration (R_h) following similar approaches described by *Kaplan* [2002] and *Pickett-Heaps et al.* [2010]. The wetland CH_4 flux E [Tg CH_4 grid cell^{-1} month^{-1}] at each 0.5° grid cell (x) and monthly time step (t) is $E_{(x,t)} = F_{(x)}\beta R_{h(x,t)}S_{(x,t)}$, where F (x) is an ecosystem scaling factor, and $\beta = 0.03$ mol CH_4/ mol C respired [*Christensen et al.*, 1996]. The method is a fast running algorithm suitable for long integrations and incorporation into atmospheric chemistry-climate models. Our simple model accounts for the major global processes controlling wetland CH_4 emissions (substrate available for methanogenesis, rate of microbial decomposition, wetland extent) but we do not distinguish among different transport pathways of wetland emissions (e.g., diffusion, ebullition, and plant mediated transport) whose variability is less well characterized on global scales. Although we do not explicitly model water table position, we constrain inundated area using remote sensing observations, which allows wetland extent to fluctuate but limits potential wetlands to those areas where inundation has been observed. By calibrating our model with regional observations, we are able to capture the magnitude and seasonal variations typical of large-scale wetland CH_4 emissions.

[6] R_h was calculated using the LPJ dynamic global vegetation model [*Sitch et al.*, 2003; *Gerten et al.*, 2004]. We prescribed gridded monthly climatology from the CRU TS3.0 data set [*Mitchell and Jones*, 2005]. Non-gridded annual CO_2 concentrations were derived as in *Sitch et al.* [2003]. Following a 1000-year spin up to equilibrate vegetation and carbon pools, a transient simulation, with fire effects removed, was run for the years 1901–2005. The temperature dependence of methanogenesis is implicitly modeled through LPJ R_h using a modified Arrhenius equation [*Sitch et al.*, 2003].

[7] We created a monthly varying wetland extent product by empirically fitting the volume of water runoff simulated by LPJ to inundated area derived from multiple satellite products for 1993–2000 [*Prigent et al.*, 2007]. To fit the satellite data to the simulated runoff, we used a two-tier

---

[1]Swiss Federal Research Institute WSL, Birmensdorf, Switzerland.
[2]LERMA, CNRS, Observatoire de Paris, Paris, France.
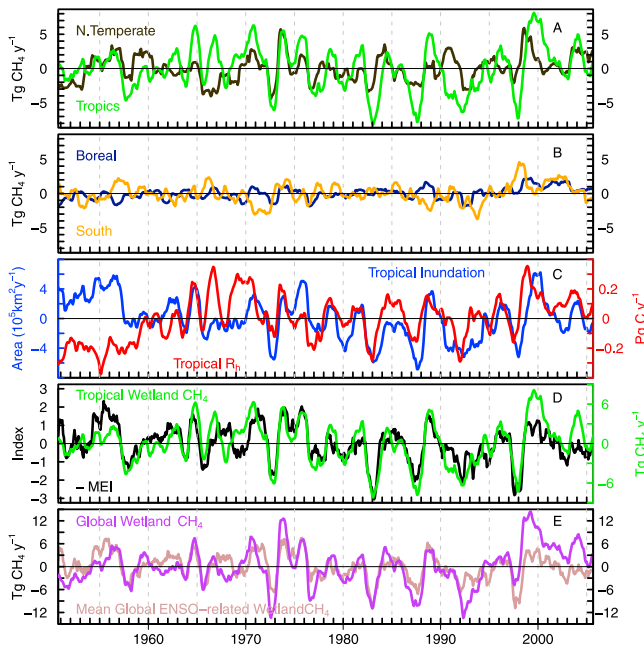[3]ARVE Group, EPFL, Lausanne, Switzerland.

Figure 1. (a and b) Regional wetland CH_4 emission anomalies from 1950–2005. Regions are grouped continental regions from the TransCom3 experiment [*Gurney et al.*, 2000]. Boreal = North American and Eurasian boreal and Europe; N.Temperate = North American and Eurasian temperate; Tropics = South American tropical, northern Africa, and tropical Asia; South = South American temperate, southern Africa, and Australia. (c) Tropical model components. (d) Tropical wetland CH_4 anomalies plotted against the negative multivariate ENSO index (−MEI). (e) Global wetland CH_4 anomalies and the calculated mean global wetland CH_4 response to ENSO. The plot ranges for Figures 1c and 1d are 3× standard deviation of each time series, which is equivalent to normalizing the time series in each panel.

approach in which we either fit linear equations by grid cell and by month or used annual regional fits created by aggregating the two data sets by TransCom land region [*Gurney et al.*, 2000] (see auxiliary material). For the North American and Eurasian boreal TransCom land regions, instead of regional fits, we used mean monthly gridded inundated area from *Prigent et al.* [2007]. Rice growing regions were excluded from the analysis [*Matthews and Fung*, 1987]. Each of the fitting methods captured approximately 50% of the inundation variability. Because boreal inundation has a large seasonal cycle, but relatively small interannual variability, we found that using mean monthly inundation for subsets of the boreal region had little impact on how well our parameterization fit the observed inundation (see auxiliary material).[1] The time series is available upon request.

[8] To account for broad ecosystem differences in CH_4 emitting capacity between tropical and boreal wetlands, we scaled R_h and S through a combination of two latitudinal scaling factors (F_T and F_B) and surface temperature. The

combined scaling factor $F(x) = \sigma_{(x)}F_T + (1 - \sigma_{(x)})F_B$, where $\sigma = \exp(T_{(x)} - T_{max})/$, $T_{(x)}$ is the mean near-surface temperature between 1960–1990, and $T_{max} = 303.35$ K. F_T and F_B were fit to match regional estimates of wetland CH_4 fluxes for the Hudson Bay Lowlands ($F(x) = 2.3$ Tg CH_4 y^{-1} [*Pickett-Heaps et al.*, 2010]) and the Amazon Central Basin ($F(x) = 9.1$ Tg CH_4 y^{-1} [*Melack et al.*, 2004]), resulting in $F_T = 0.175$ and $F_B = 0.025$ and mean global emissions of 171.2 Tg CH_4 y^{-1} over 1950–2005.

[9] We used the multivariate ENSO index (MEI) to represent ENSO strength because the index integrates multiple climate variables, and is thus suited for a global analysis of climate-land-atmosphere interactions [*Wolter and Timlin*, 1998]. The negative MEI closely follows the more commonly used Southern Oscillation index. MEI has a 3-month lag compared to major global precipitation events in the input CRU TS3.0 data, thus, we lagged our wetland model output by 3 months (see auxiliary material).

[10] For the following analysis, we used anomalies exclusively. Wetland CH_4, inundation, and R_h anomalies were calculated by subtracting 1950–2005 monthly means, averaging over 2 successive months to match MEI, which is a bimonthly index, and by smoothing with a 12-month running mean. Our modeled interannual variability is generally within uncertainty ranges from inverse flux estimates (*Bousquet et al.* [2006] and auxiliary material), especially considering possible overestimates in the global OH variability used for *Bousquet et al.*'s [2006] inversions [*Montzka et al.*, 2011]. We improve model agreement with inverse estimates compared to LPJ CH_4 model versions with no dynamical wetland extent [*Spahni et al.*, 2011].

3. Results and Discussion

[11] We find that the majority of interannual variability in global wetland CH_4 emissions stems from variability in the tropics (44%) and northern temperate (27%) regions (as defined in Figure 1). Boreal (12%) and southern (18%) regional variability are smaller fractions of the global total (Figures 1a and 1b). Variability in tropical wetland CH_4 emissions is due more to variations in inundated area than soil carbon content ($R^2_{inundation} = 0.65$, $R^2_{Rh} = 0.39$; Figure 1c), while the reverse is true for the boreal region ($R^2_{inundation} = 0.16$, $R^2_{Rh} = 0.77$; not shown). Similarly, *Bloom et al.* [2010] find that variations in precipitation explain more of the tropical CH_4 variability than temperature, whereas temperature variations are a better indicator of CH_4 variability at higher latitudes.

[12] The majority of modeled tropical wetland variability matches the phasing and amplitude of the negative multivariate ENSO index (−MEI, Figure 1d). Thus, tropical wetland CH_4 emission anomalies are well correlated with

Table 1. Mean Global Wetland CH_4 Response to ENSO Summed by Decade

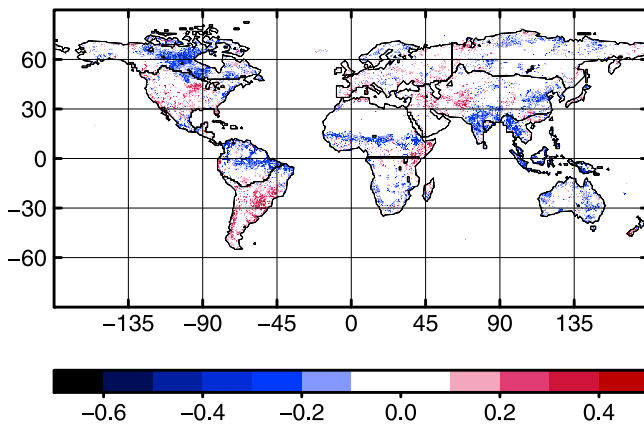| Decade	Anomalies (Tg CH_4)
1950–59	11
1960–69	7
1970–79	11.5
1980–89	−10
1990–99	−16
2000–05	−2

Figure 2. Grid cell partial correlations ($p < 0.05$) between the multivariate ENSO index (MEI) and modeled wetland CH_4 emissions from 1950–2005.

MEI ($R^2 = 0.56$). Because tropical variability is the largest fraction of global variability, global wetland CH_4 variability is also well correlated with MEI ($R^2 = 0.39$, not shown). These results suggest that ENSO has a significant effect on not only tropical but also global wetland emissions.

[13] To isolate the effect of strong ENSO years on wetland CH_4 emissions, we calculated the average wetland CH_4 anomalies for those ENSO years that occur in the top and bottom quartile of the MEI (6 El Niño (1957, 1965, 1972, 1982, 1986, 1997) and 7 La Niña events (1954, 1964, 1970, 1973, 1975, 1988, 1998)). We did not include the 1991–93 El Niño because of the influence of the Mt. Pinatubo eruption during that period. We estimate a maximum and mean decrease of -13 Tg CH_4 y^{-1} (1972–74 El Niño) and -9 ± 3 Tg CH_4 y^{-1} during El Niño years; and a maximum and mean increase of $+14$ Tg CH_4 y^{-1} (1998–2000 La Niña) and $+8 \pm 4$ Tg CH_4 y^{-1} during La Niña years.

[14] Compared to estimates of interannual variability in global biomass burning, it seems likely that ENSO has caused greater variation in CH_4 emissions from wetlands than from fires in recent decades. Mean biomass burning anomalies estimated by *Bousquet et al.* [2006] are $\sim \pm 4$ Tg CH_4 y^{-1} for those ENSO events listed above that fall within their study period (1985–2004). This is approximately half of the mean response, that we calculate for wetlands during ENSO events. *van der Werf et al.* [2006] calculate maximum anomalies of $+9$ Tg CH_4 y^{-1} from biomass burning for both the largest recorded El Niño event in 1997 and during the subsequent 1998 La Niña year, hinting at possible anti-correlations between wetland and biomass burning anomalies during ENSO years.

[15] The strength and frequency of El Niño or La Niña events varies depending on the decade. Since MEI is well correlated with wetland CH_4 variability and wetland emissions are thought to be the major source of interannual variability in atmospheric CH_4 concentrations [*Bousquet et al.*, 2006], it seems likely that ENSO variability may also have had an influence on the growth rate, or rate of accumulation, of CH_4 in the atmosphere. To test this, we created a mean ENSO response curve based on linear regressions of wetland CH_4 variability with MEI (Figure 1e) (i.e., January 2000 ENSO-related anomalies are $\sum_{i=1-11} (m_i \times MEI + b_i)_{01/2000}$

where i represents one of 11 land regions [*Gurney et al.*, 2000] and m and b are the regional monthly regression ($p < 0.05$, $n = 672$) slope and intercept, respectively. When the mean response curve is summed by decade, we see that ENSO can increase or decrease decadal wetland CH_4 emissions by up to 16 Tg CH_4 (Table 1). Global CH_4 emissions from all anthropogenic sources [*Joint Research Centre and Netherlands Environmental Assessment Agency*, 2010] slowed from a rapid increase of approximately $+190$ Tg CH_4/decade during the 1970s to $+60$ and -20 Tg CH_4/decade during the 1980s and 1990s, respectively." Past studies have found that the slow down in the CH_4 growth rate, observed over the last several decades until very recently [*Rigby et al.*, 2008], can be attributed to changes in anthropogenic emissions [*Wang et al.*, 2004; *Bousquet et al.*, 2006]. We estimate that a decrease of -49 Tg CH_4 from wetlands during 1980–99 relative to the $+11.5$ Tg CH_4 increase in the 1970s (Table 1) due to stronger El Niño than La Niña events contributed an additional $\sim 14\%$ to the slow down in CH_4 emissions compared to anthropogenic sources.

[16] Grid cell correlations between MEI and modeled wetland CH_4 emission anomalies are presented in Figure 2. Agreement is not as strong as for the continental regions in Figure 1, but the grid cell correlations highlight regional differences. Positive variations in MEI (or the El Niño state) are most strongly linked to lower wetland CH_4 emissions across the tropics and in boreal North America and higher emissions in temperate South America. The inverse correlation in both the tropics and North American boreal regions has interesting potential consequences. The present day effect of ENSO on wetland CH_4 emissions is dominated by the ENSO-wetland relationship in the tropics, with some opposing effect from oppositely correlated temperate regions. If CH_4 emissions continue to increase from the boreal region as projected [*Zhuang et al.*, 2006; *McGuire et al.*, 2010] leading to likely increases in interannual variability from the boreal region, our results suggest this would further strengthen ENSO's effect on global wetland methane variability, with larger negative anomalies during El Niño phases and larger positive anomalies in La Niña years.

4. Conclusions

[17] Our results show that global wetland CH_4 variability is strongly related to ENSO variability. Thus, future ENSO variations and trends will likely have a significant impact on global atmospheric CH_4 concentrations. The tropics contribute almost half of the global interannual variability, which makes both improving our process knowledge of tropical wetland methane emissions at regional scales (e.g., from flux-tower and aircraft measurements), and better constraining potential future trends in tropical climate, especially precipitation, an important criteria for projecting the future of the global CH_4 budget. A future climate more like the El Niño state will decrease global wetland CH_4 emissions, while the reverse is true for a future climate more like the La Niña state. Over the last three decades, the trend towards more El Niño events has decreased wetland CH_4 emissions compared to the previous three decades before 1980. While more work is needed to isolate the interaction of other CH_4 sources and sinks affected by ENSO variability, namely biomass burning and OH variability, it seems likely

that the effect of ENSO on wetland emissions is partly responsible for the stabilization of the atmospheric growth rate of CH_4 over recent decades.

References

Bloom, A. A., P. I. Palmer, A. Fraser, D. S. Reay, and C. Frankenberg (2010), Large-scale controls of methanogenesis inferred from methane and gravity spaceborne data, *Science*, 322, 322–325, doi:10.1126/science.1175176.

Bousquet, P., et al. (2006), Contribution of anthropogenic and natural sources to atmospheric methane variability, *Nature*, 443(7110), 439–443, doi:10.1038/nature05132.

Chen, Y. H., and R. G. Prinn (2006), Estimation of atmospheric methane emissions between 1996 and 2001 using a three-dimensional global chemical transport model, *J. Geophys. Res.*, 111, D10307, doi:10.1029/2005JD006058.

Christensen, T. R., I. C. Prentice, J. Kaplan, A. Haxeltine, and S. Sitch (1996), Methane flux from northern wetlands and tundra, *Tellus, Ser. B*, 48, 652–661, doi:10.1034/j.1600-0889.1996.t01-4-00004.x.

Dlugokencky, E. J., et al. (2009), Observational constraints on recent increases in the atmospheric CH_4 burden, *Geophys. Res. Lett.*, 36, L18803, doi:10.1029/2009GL039780.

Gerten, D., S. Schaphoff, U. Haberlandt, W. Lucht, and S. Sitch (2004), Terrestrial vegetation and water balance—Hydrological evaluation of a dynamic global vegetation model, *J. Hydrol.*, 286, 249–270, doi:10.1016/j.jhydrol.2003.09.029.

Gurney, K., R. Law, P. Rayner, and A. S. Denning (2000), TransCom 3 experimental protocol, *Pap. 707*, Colo. State Univ., Fort Collins. [Available at http://www.purdue.edu/transcom/transcom03_protocol.php.]

Joint Research Centre and Netherlands Environmental Assessment Agency (2010), Emission Database for Global Atmospheric Research (EDGAR), release version 4.1, http://edgar.jrc.ec.europa.eu, Eur. Comm., Ispra, Italy.

Kaplan, J. (2002), Wetlands at the last glacial maximum: Distribution and methane emissions, *Geophys. Res. Lett.*, 29(6), 1079, doi:10.1029/2001GL013366.

Matthews, E., and I. Fung (1987), Methane emissions from natural wetlands: Global distribution, area, and environmental characteristics of sources, *Global Biogeochem. Cycles*, 1(1), 61–86, doi:10.1029/GB001i001p00061.

McGuire, A. D., et al. (2010), An analysis of the carbon balance of the Arctic Basin from 1997 to 2006, *Tellus, Ser. B*, 62, 455–474, doi:10.1111/j.1600-0889.2010.00497.x.

Melack, J. M., et al. (2004), Regionalization of methane emissions in the Amazon Basin with microwave remote sensing, *Global Change Biol.*, 10, 530–544, doi:10.1111/j.1365-2486.2004.00763.x.

Mitchell, C., and P. Jones (2005), An improved method of constructing a database of monthly climate observations and associated high-resolution grids, *Int. J. Climatol.*, 25, 693–712, doi:10.1002/joc.1181.

Montzka, S. A., M. Krol, E. Dlugokencky, B. Hall, P. Jöckel, and J. Lelieveld (2011), Small interannual variability of global atmospheric hydroxyl, *Science*, 331, 67–69, doi:10.1126/science.1197640.

Pickett-Heaps, C. A., et al. (2010), Magnitude and seasonality of wetland methane emissions from the Hudson Bay lowlands (Canada), *Atmos. Chem. Phys. Discuss.*, 10(9), 22,415–22,435, doi:10.5194/acpd-10-22415-2010.

Prigent, C., F. Papa, F. Aires, W. B. Rossow, and E. Matthews (2007), Global inundation dynamics inferred from multiple satellite observations, 1993–2000, *J. Geophys. Res.*, 112, D12107, doi:10.1029/2006JD007847.

Rigby, M., et al. (2008), Renewed growth of atmospheric methane, *Geophys. Res. Lett.*, 35, L22805, doi:10.1029/2008GL036037.

Ringeval, B., N. de Noblet-Ducoudré, P. Ciais, P. Bousquet, C. Prigent, F. Papa, and W. B. Rossow (2010), An attempt to quantify the impact of changes in wetland extent on methane emissions on the seasonal and interannual time scales, *Global Biogeochem. Cycles*, 24, GB2003, doi:10.1029/2008GB003354.

Shindell, D. T., G. Faluvegi, D. M. Koch, G. A. Schmidt, N. Unger, and S. Bauer (2009), Improved attribution of climate forcing to emissions, *Science*, 326, 716–718, doi:10.1126/science.1174760.

Sitch, S., et al. (2003), Evaluation of ecosystem dynamics, plant geography and terrestrial carbon cycling in the LPJ dynamic global vegetation model, *Global Change Biol.*, 9, 161–185, doi:10.1046/j.1365-2486.2003.00569.x.

Spahni, R., et al. (2011), Constraining global methane emissions and uptake by ecosystems, *Biogeosciences Discuss.*, 8, 221–272, doi:10.5194/bgd-8-221-2011.

van der Werf, G. R., et al. (2006), Interannual variability in global biomass burning emissions from 1997 to 2004, *Atmos. Chem. Phys.*, 6, 3423–3441, doi:10.5194/acp-6-3423-2006.

Walter, B. P., M. Heimann, and E. Matthews (2001), Modeling modern methane emissions from natural wetlands: 2. Interannual variations 1982–1993, *J. Geophys. Res.*, 106(D24), 34,207–34,219, doi:10.1029/2001JD900164.

Wang, J. S., J. A. Logan, M. B. McElroy, B. N. Duncan, I. A. Megretskaia, and R. M. Yantosca (2004), A 3-D model analysis of the slowdown and interannual variability in the methane growth rate from 1988 to 1997, *Global Biogeochem. Cycles*, 18, GB3011, doi:10.1029/2003GB002180.

Wolter, K., and M. Timlin (1998), Measuring the strength of ENSO events: How does 1997/98 rank?, *Weather*, 53(9), 315–324.

Zeng, N., A. Mariotti, and P. Wetzel (2005), Terrestrial mechanisms of interannual CO_2 variability, *Global Biogeochem. Cycles*, 19, GB1016, doi:10.1029/2004GB002273.

Zhuang, Q., J. M. Melillo, M. C. Sarofim, D. W. Kicklighter, A. D. McGuire, B. S. Felzer, A. Sokolov, R. G. Prinn, P. A. Steudler, and S. Hu (2006), CO_2 and CH_4 exchanges between land ecosystems and the atmosphere in northern high latitudes over the 21st century, *Geophys. Res. Lett.*, 33, L17403, doi:10.1029/2006GL026972.

E. L. Hodson, B. Poulter, and N. E. Zimmermann, Swiss Federal Research Institute WSL, Zuercherstrasse 111, CH-8903 Birmensdorf, Switzerland. (elke.hodson@wsl.ch)

J. O. Kaplan, ARVE Group, EPFL, Station 2, CH-1015 Lausanne, Switzerland.

C. Prigent, LERMA, CNRS, Observatoire de Paris, 61, Avenue de l'Observatoire, F-75014 Paris CEDEX, France.